An Approach for the Retrieval of Land Surface Temperature from the Industrial Area Using Landsat-8 Thermal Infrared Sensors

An Approach for the Retrieval of Land Surface Temperature from the Industrial Area Using Landsat-8 Thermal Infrared Sensors

M Z Dahiru[1,2,3,] Mazlan Hashim[1, 2*]
[1]Geoscience & Digital Earth Centre (INSTEG), Research Institute for Sustainable Environment (RISE), Universiti Teknologi Malaysia, Johor Bahru, Malaysia
[2]Faculty of Geoinformation & Real Estate, Universiti Teknologi Malaysia, Johor
[3]Adamawa State Polytechnic, Yola. Adamawa State Nigeria

*E-Mail: mazlanhashim@utm.my

Abstract: The thermal imagine provides data with synoptic coverage for investigating thermal information from hot sources for detecting, mapping energy loss from the industrial area. This study attempts to retrieved heat loss from the industrial area using Landsat-8 TIRS experimented at an industrial area of Pasir Gudang, Peninsular Malaysia, the main objective is to investigate the sensitivity of Landsat-8 TIR for detecting industrial thermal energy within the various range of targets of different temperatures. An estimated heat map with absolute surface temperature values is the final output. Apart of the pre-processing of Landsat-8 TIRS data, data are processed for the retrieval of land surface temperature, then subjected to a downscaling process to final 30 x 30 m pixels, hence enable to merge with all Landsat-8 bands for visualization and validation of results. The split window algorithm (SWA) is used for the temperature retrieval from band 10 and 11, with other driven parameters. The Multiple Adaptive Regression Splines (MARS) model for spatial downscaling was adopted in this study. The generated thermal energy map was then validated over selected targets in the field and compared to corresponding downscaled MODIS LST product (MODIS11A2). TIR bands applied with SWA generated 13.7°C temperature dynamic range from 22.35~51.36° C in comparison with MODIS LST product values range from 27.17 ~ 37.65°C). Results indicated good agreement between the generated thermal energy map with the in-situ validations (RMSE=0.43 °C). It is therefore concluded that derived Land surface temperature map derived is suitable for study industrial thermal environment at 1:50,000 ~ 100,000 scales, adequately to be used for environmental impact assessment.

Keywords: Remote sensing, **s**plit-window algorithm, downscaling.

1. Introduction

Thermal imagine is an authoritative means for exploding the thermal information used to repossess LST [1]. Cognition of the LST is an indicator that can offer valuable data from the various geophysical environmental application (geological studies, mineral exploration and evapotranspiration)[2, 3]. Consequently, The advancement in remote sensing technology offers an opportunity to provide a reliable, consistent and repeatable approach within the working frame from local to a global scale, as well as long term monitoring oil spillage operations [4, 5]. The development and changes related to land cover and urban features have been associated with industrial heat emission, where the surface air

temperature is becoming higher compared to the surrounding environment [6]. There is a need for industrial heat regulations which will attach to green space to monitor the heat intensity from industrial heat emissions through a descriptive technology [7, 8] In connection with ground truth measurement of air temperature [9]**.**

Therefore, the study of LST contributes in identifying the extent of high temperature from the thermal information over the different urban land cover boundary which limited to a comparatively small area in which concurrently measured air temperature through the full stretch. Thus, the remotely sensitively approached for LST offered an option to capture the relatively small area as good as a larger area. However, the special solution for such datasets which ranging from 60m to 100m TIRS and 1000 m MODIS product is insufficient to capture a little lot of industries that emit heat in relation heterogeneous ground features [10]. Established in the preview literature on prominent research, downscaling studies of coarse spatial resolution LST of the developed areas were relatively targeted with final downscaling special resolution comprising 1000 m, 480-120m, 6m-90m, 50m, and 30m [11-15] with downscaling factors, recently attempt on downscaling to 2m special resolution.

In this paper, we apply medium resolution data from Landsat 8 TIR bands (10 and 11) to generate LST image for Pasir Gudang industrial area based on the relationship with MODIS product data, which the technique for multiple adaptive regression splines (MARS) was tested to suit diverse regression function into different n-dimensional data [12]. Nevertheless, the MARS techniques predict the special distribution of environmental activities, mostly limited to soil mapping [13] and landslide detection [14]. Therefore, we undertake to use MARS in LST downscaling for the industrial area of Pasir Gudang. The objectives of this study present as follow; (i) To explore the techniques for downscaling spatial resolution images for both Landsat-8TIRS and MODIS LST product for enhancing the accuracy of the downscaled map (ii) to investigate the sensitivity of Landsat-8 TIR for detecting industrial thermal energy heat emission within various range of targets for different temperatures (iii) and to evaluate the link between the industrial material and thermal energy at microscales (1:50,000 ~ 100,000 scales) [18, 19]. Therefore, the potential of Multivariate Adaptive Regression Splines model is suitable for study industrial thermal energy for impact assessment. Therefore, detecting, mapping, and monitoring of industrial heat energy sources to support understanding toward improving disparities on existing industrial substances for policymaker's implementation.

2. Study Area

Pasir Gudang industrial is one of the large leading industrial estate located in Iskandar Johor, peninsular Malaysia at large, which located between latitude 1° 30'10''N and 103° 56'8'' E, with the approximate total area of 359.57 Km2 (138.83 sqm) with an approximate population of about 46,571 to a density of 130 km2 (340/sqmi) Figure 1[17].

The major energy sources include the primary fuel gas and the secondary fuel oil, which recognized as the biggest gas turbine power station in Malaysia. The temperature of the study area is influenced by the two main seasons; Winter period (Northeast monsoon) brings heavy rainfall mostly to the east coast states during November to March, and Summer period (Southwest monsoon) signifies relatively with drier weather during May to September [18].

3. Material and Method

In this study, satellite-based data from Landsat 8 TIRS and MODIS LST product shown in (Table 1) was acquired. The satellite data was taken in the perspective of exertion along with the account of LST for which summer acquisition date to be free cloudy image [19]. However, there is a large uncertainty from TIR band 11 from Landsat 8, [20] thereby choose to use both TIR band 10 and 11 as a single spectral band for the retrieval of LST using the split-window algorithm [21]. The data taken from two different sensors were processed in a multi-software program (ArcGis10.5 and Erdas imagine 2014) for the analysis. Therefore, this paper intended to test the ability of TIR sensors from Landsat-8 to records LST from Pasir Gudang industrial area. To achieve these objectives, the following steps were actualized

shown in 'figure 2' pixels values conversion of TIRS bands to TOA spectral radiance, then to brightness atmospheric temperature then lastly from at-satellite temperature LST through implementing the SW algorithm, and finally, the statistical analysis was carried out using regression function.

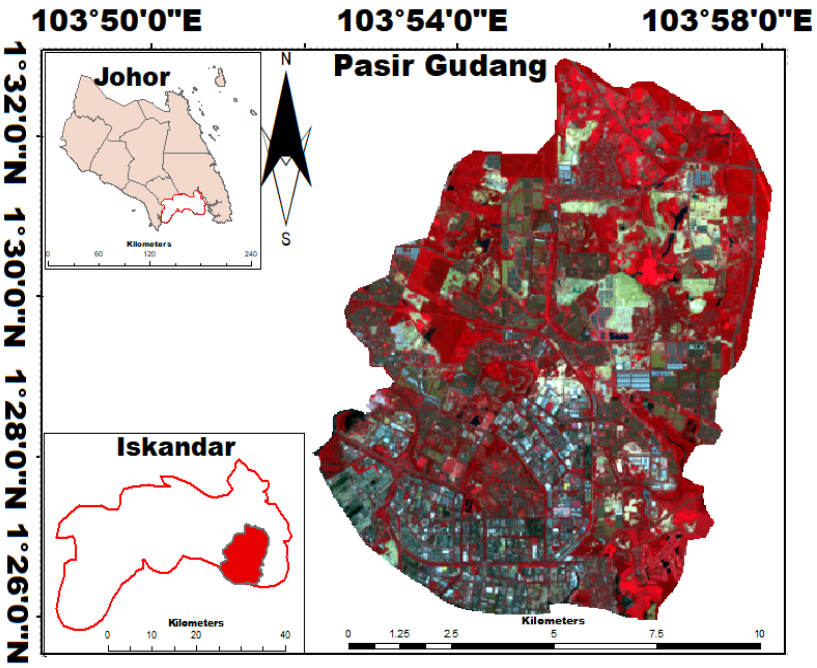

Figure 1. Location of the study area.

3.1 Conversion of digital number (DN) to radiance

The top of atmospheric (TOA) of the OLI band (2-7) and TIRS sensor band (10 and 11) are estimated separately. The sensor converts a raw image into the spectral radiance, the equation is realized using ArcGIS 10.5 software package

$$L_\lambda = M_L \times \varphi_{cal} + A_L - Q_i \quad (1)$$

where, L_λ is the TOA spectral radiance (watts/(m^2srad $*$ µm)) ; M_L – band-specific multiplicative rescaling factor obtained from the metadata Table 3 [22].

3.2 Conversion to at satellite Brightness temperature (BT)

BT is the electromagnetic radiance moving upward from the top of earth's atmosphere to allow the thermal calibration conversion (The DN values of TIR band 10 and 11 to TOA spectral radiance), (USGS Handbook, 2013) equation 1. therefore, The BT is not a temperature on the ground rather is the temperature at the satellite.

$$T_B = \frac{K_2}{Ln\left[\left(\frac{K_1}{L_\lambda}\right)+1\right]} - 273.15 \quad (2)$$

where: T_B- At satellite brightness temperature (K); K_1-Calibration constant 1 (watts/(m^2srad $*$ µm); K_2 -Calibration constants 2, However, the values are in Kelvin (K), to have it in Celsius degree, it is necessary to consider by adding absolute zero which is equal to -273.15.

Table 1. Specification of the data used in the study.

Sensors	Bands	SR	Path/Row	Date
TIR band (10 & 11)	TIRS bands (10,11), OLI (5,4)	100m	125/59	24/5/2018
MODIS/MOD11A2	TIRS bands (31,32)	1000m	MOD21_L2 Terra	24/05/2018

3.3 Land surface Emissivity

Accurate LST estimation from TIR bands (10 and 11) rely on atmospheric effect features with adequate knowledge of LSE [23]. The LSE and LST are two substantial variables used to identified land surface processes and charge of radiation budget. Therefore, this paper, the NDVI-based emissivity process was implemented to estimate the NDVI derived from TIR bands (10 and 11) data. The NDVI was categorised into bare soil ($NDVI < 0.2$), mixture of bare soil and vegetation ($0.2 \leq NDVI \leq 0.5$), and fully vegetation ($NDVI > 0.5$), each of these classes is estimating using the following equation [27, 28].

$$\mathrm{FVC} = [\frac{(NDVI - NDVI_{min})}{(NDVI_{max} - NDVI_{min})}]^2 \quad (3)$$

$$\varepsilon_\lambda = \varepsilon_{v\lambda} FVC + \varepsilon_{s\lambda}(1 - FVC) + C_\lambda \quad (4)$$

Where; $\varepsilon_s \; and \; \varepsilon_v$ represents the emissivity of vegetation and soil respectively, FVC represent proportional of vegetation, and C represent the surface roughness with a constant value of 0.005 [26].

The NIR and red band used to estimate the NDVI values: This study realised the NDVI for soil as -0.334 ($NDVI_{min}$), while for vegetation as 0.6459 ($NDVI_{max}$).

$$\mathrm{NDVI} = \frac{\mathrm{NIR(band5)} - \mathrm{R(band4)}}{\mathrm{NIR(band5)} + \mathrm{R(band4)}} \quad (5)$$

3.4 LST Retrieval

The LST can be retrieved using the SW algorithm developed by [25] for Landsat -8 TIRS. According to [27], the Split-Window methods use two TIRs bands classically located in the atmospheric window between 10 and 12 μm, The mathematical structure for estimating the LST Landsat 8 can be articulated as [25, 28], expressed in Equ (6): Where T_s is given as;

$$T_{B10} + c_1(T_{B10} - T_{B11}) + c_2(T_{B10} - T_{11})^2 + \cdots$$
$$+c_0 + (c_3 + c_4 w)(1 - \varepsilon) + (c_5 + c_6 w)\Delta\varepsilon \quad (6)$$

T_s is given as Land surface Temperature; T_{B10}, T_{B11} are the Brightness temperature of band 10 and 11 of Landsat -8; TIRS W is the atmospheric water vapour contents (g/cm^2). ε mean emissivity; $\Delta\varepsilon$ emissivity differences; c_0 to c_6- is the SW coefficient values. The coefficient values for SW were shown in Table 2 [32, 33].

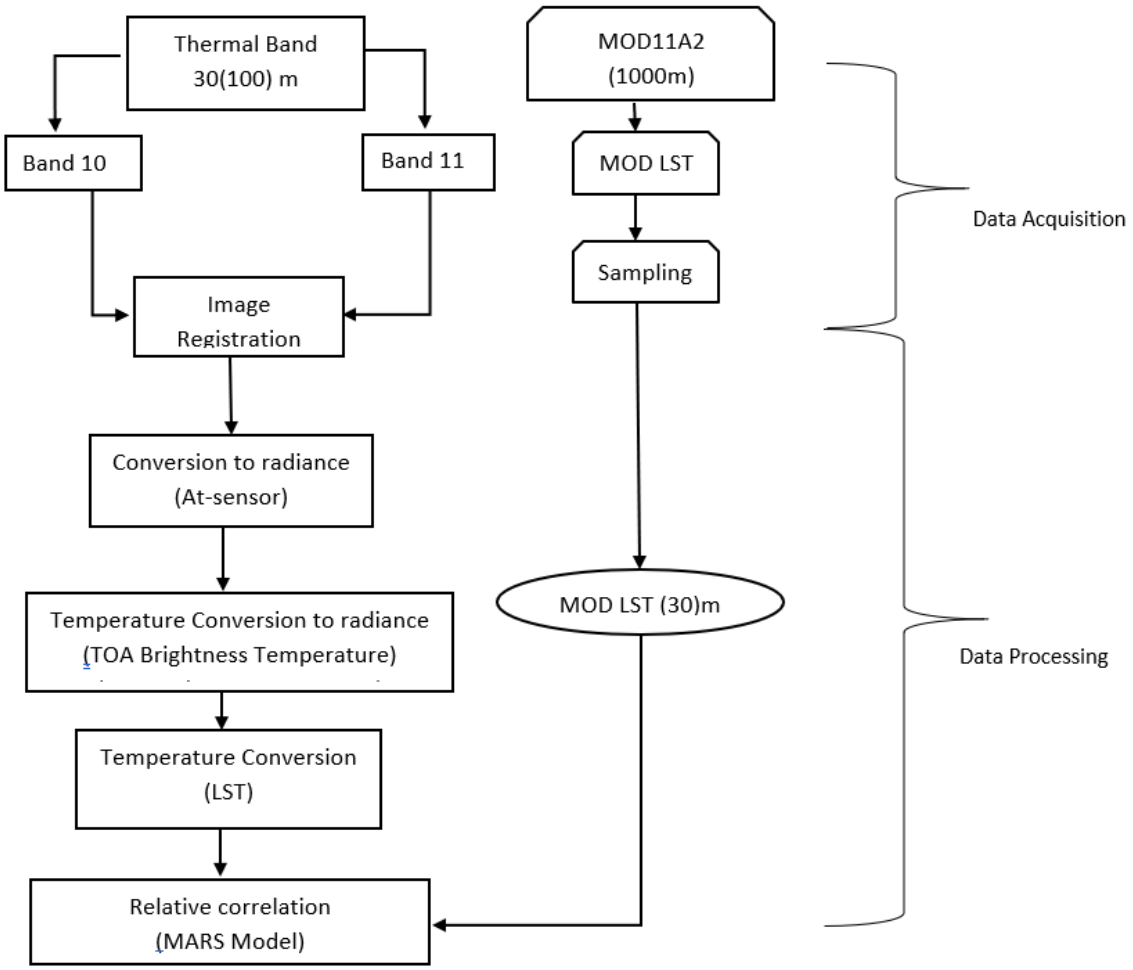

Figure 2. Methodological flowchart.

Table 2. SW coefficients values for TIRS bands of Landsat-8 imagery.

Constants	c_0	c_1	c_2	c_3	c_4	c_5	c_6
Value	-0.268	1.378	0.183	54.300	-2.238	-129.200	16.400

3.5 Verification of the results

As a result of the inaccessibility of different LST, the downscaled map was validated using the retrieved Landsat 8- TIR bands. Consequently, the developed models were proved by adjusted R^2 at the same calculate the RMSE between the derived TIRS data and downscaled LST map, RMSE was calculated in two approaches. Firstly, $RMSE_{2/4m}$ was calculated from two differences between the observed $LST_{30(100)m}$, resampled to 30m spatial resolution with the nearest neighbour method to enable the calculation presented in equation 7 and download map $LST_{MARS2/4m}$ [10].

$$RMSE_{2/4m} = \sqrt{\frac{1}{N}\sum_{i-1}^{N}(LST_{30(100)m} - LST_{\frac{MARS2}{4m}})^2} \qquad (7)$$

Therefore, $RMSE_{2/4m}$ was calculated an evaluation between Landsat8 derived map and downscaled map adjusted for residual($\Delta LST_{30(100)m}$) map $LST'_{\frac{MARS2}{4m}}$. equation (8)

$$RMSE'_{2/4m} = \sqrt{\frac{1}{N}\sum_{i-1}^{N}(LST_{30(100)m} - LST'_{\frac{MARS2}{4m}})^2} \quad (8)$$

4. Result and Discussion

The study aimed to evaluate estimated LST from Landsat TIR bands for Pasir Gudang industrial using the MODIS LST product as a prey. In context, the method being used was highlighted for retrieving LST; the retrieved LST from Landsat-8 was compared with MODIS derived-LST, which covers entire Peninsular Malaysia daily in three MODIS thermal infrared bands (29, 31, and 32) at a spectral resolution of 1000 m at nadir, which spans from 3.66 to 14.28 microns. The images used in the study have different standards, with a spatial resolution of 1000m for MODIS and 100m for Landsat-8 TIR. Therefore, MODIS LST product with 1000m was resembled 500 m before the integration using ArcGIS 10.5 software 'figure 3'. Thus, the two LST distributions are reliable, the retrieved LST range from 22.36°C to 51.36°C with a mean of 36.85°C. Though, the retrieved MODIS LST values are far less than that of Landsat-8 with the variation of 13.71°C (Landsat-8 _LST 22.36 to 51.36°C and MOD_LST 27.17°C to 37.65°C). This is attributed as a result of; (i) Existed time variation of 30 min. between the sensors as well as rapid changes in LST of impervious surfaces caused by the high reflectivity from thermal objects,(ii) the contents of water vapour parameter in producing MODIS LST product is received by their difference between channels,(iii) Reassembled the spatial resolution of retrieved LST from 100 m to 500 m result in the extend of a scaled effect [32]. The linear regression plots were realised using 55 samples from the comparative values to validate and analyse the relationship between the two different sensors used (MODIS LST product and TIR bands 10 and 11). Therefore, the statistical model indicates shown in 'figure 5' indicate the correlation coefficient as R^2 0.78, and 0.82, which shows the significant positive correlation between retrieved LST from Landsat-8 using split-window algorithm and MODIS LST data product provided by the USGS through NASA.

The statistical analysis of the LST value of the Pasir Gudang industrial area in 2018 (Table 4) shows a correlation between land cover and the estimated LST. The industrial area has the highest LST, and Agricultural activities have the lowest LST. The average LST value of the 1ndustrial area is 37.33°C and for Agricultural activity is 30.19°C. The greenness areas have a lower LST average compared to the developed area (industrial and built-up area). Therefore, this survey suggests the existence of vegetation and the land cover be imputed to the decrease of LST in the study areas.

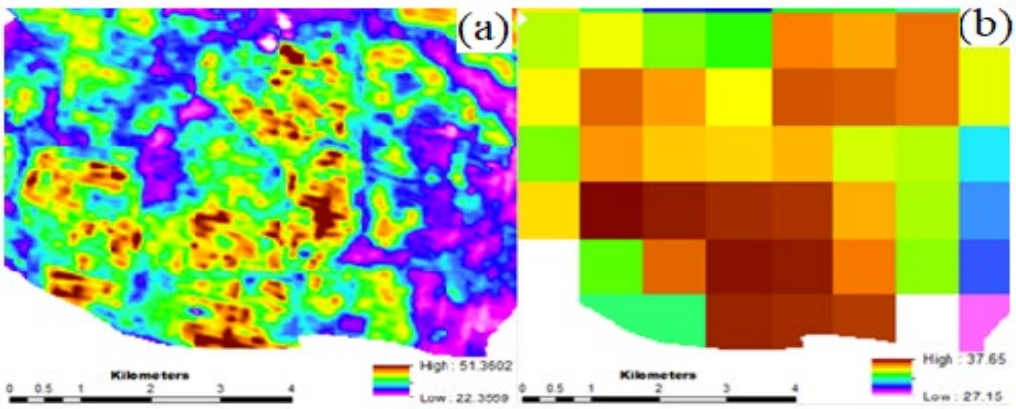

Figure 3. Retrieved LST (a) Landsat-8 (b) MODIS LST product.

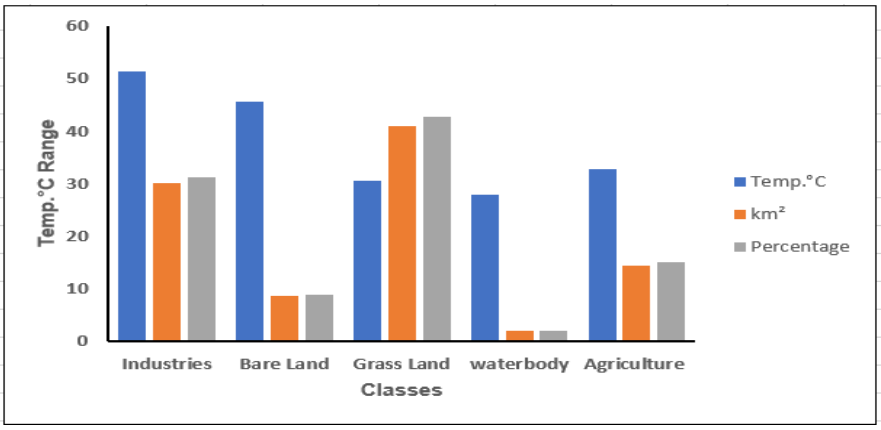

Figure 4. The histogram distribution of features classes in Pasir Gudang industrial area.

Table 3. Statistical features of LST values in Pasir Gudang industrial area.

Class	Area	Percentage	Emissivity	NDVI	Max	Std
Industries	3007.890	31.323	0.994	0.101	51.360	3.140
Bare Land	855.630	8.912	0.995	0.204	45.581	2.307
Grass Land	4101.482	42.710	0.991	0.435	30.671	2.922
waterbody	196.741	2.052	0.990	0.135	28.026	3.595
Agriculture	1441.173	15.013	0.991	0.646	32.820	1.355

The highest LST values were mostly set up in the industrial hotspot sources. The greenest area covers the dominant part with 42.7%. In disparity, agricultural activity area was set up with the minimum LST of about 32.82°C. The correlation of NDVI and LST distribution expressed by the linear correlation 'figure 5'. The result indicates the relationship between NDVI and retrieved TIRS LST has a negative correlation, well corresponds with another report [32, 33] which indicate that the vegetation area was useful for decreasing LST, there will be comfortability in an area with law LST when compare with higher LST.

In this context, we demonstrated the priority on thermal waste heat changes in Pasir Gudang industrial area based on LST information. The highest significance is indicating red colour which is a high significance covered 30.1% has a great LST value range (LST> 50 °C). The second significance with yellow included 8.9% has an LST value (LST> 40 °C). While the third priority, indicating with green colour consists of 42.71% has an LST value (LST> 30 °C). 'figure 6'. The highest LST was traced in the industrial area, which barren land was mostly found, and the lowest temperature is marked in the highly elevated areas with dense vegetation cover. Similarly, moderate temperatures are apprehending social collective from the environment and public amenities.

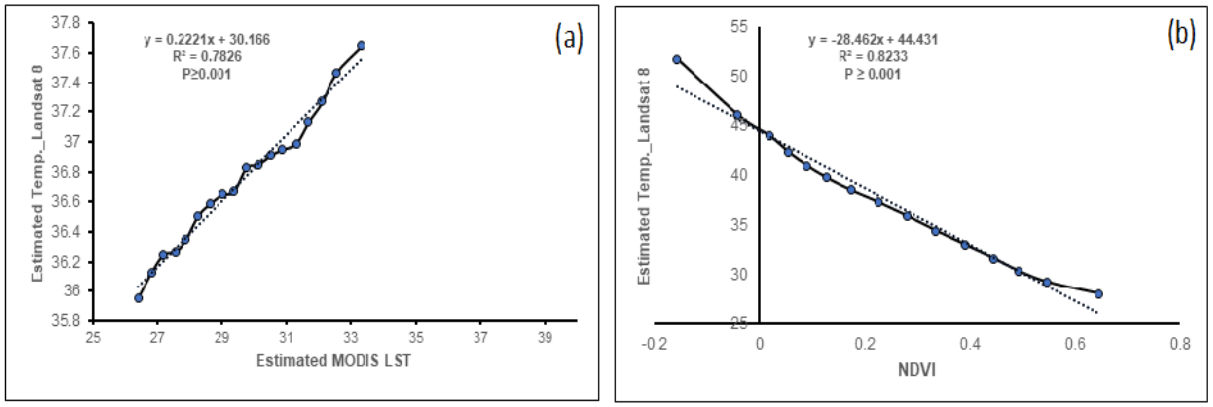

Figure 5. (a) Linear plots of retrieved LST from TIR band 10 & 11 with MODIS LST product (b) Linear plots analyses of retrieved TIRS LST and NDVI.

Some major heat source emission can be easily distinguished as shown in 'figure 6'. The strong hotness of these classes was caused by an industrial emission and other artificial surfaces (asphalt, roof sheeting, etc.). Furthermore, surrounding features (empty land, sandstones) other features of LST emissions from the industrial area and the bare land nearby has LST>35°C, due to specific thermal properties and thermal inertia [35]. Besides, when bare land surface exposed to solar radiation warms up very rapidly between 08:00 and 12:00, which contrasts with the city and these areas significantly visible [36]. As well, the effect of Temperature on trees was attributed to two factors such as direct shading and evapotranspiration cooling [37].

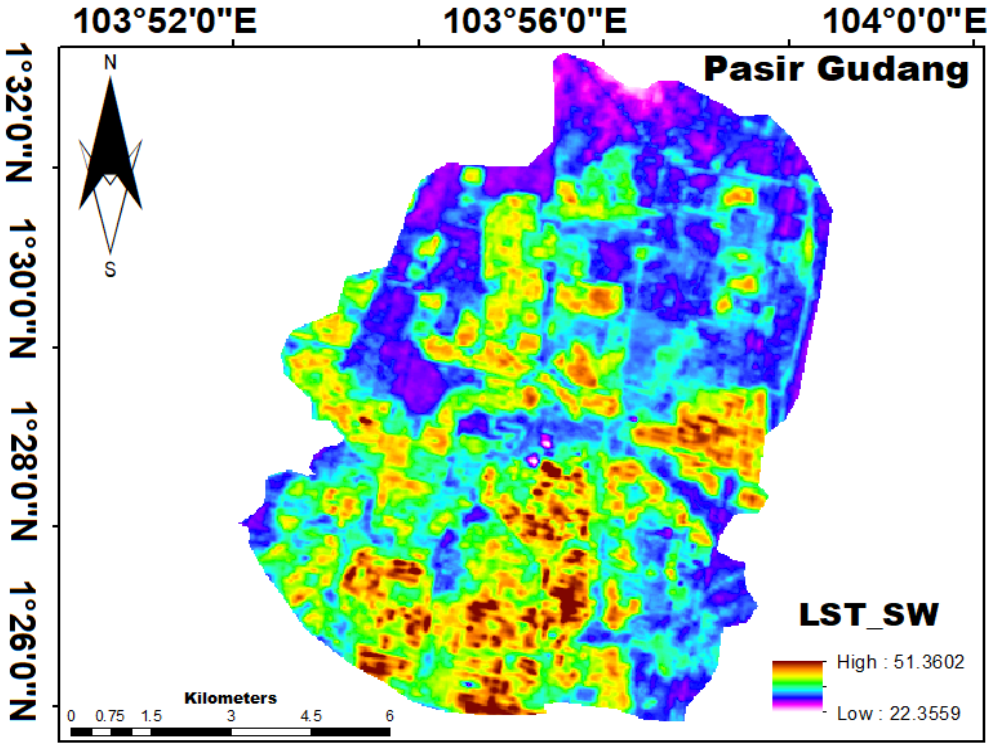

Figure 6. The retrieved LST using split-window algorithm of Pasir Gudang industrial area.

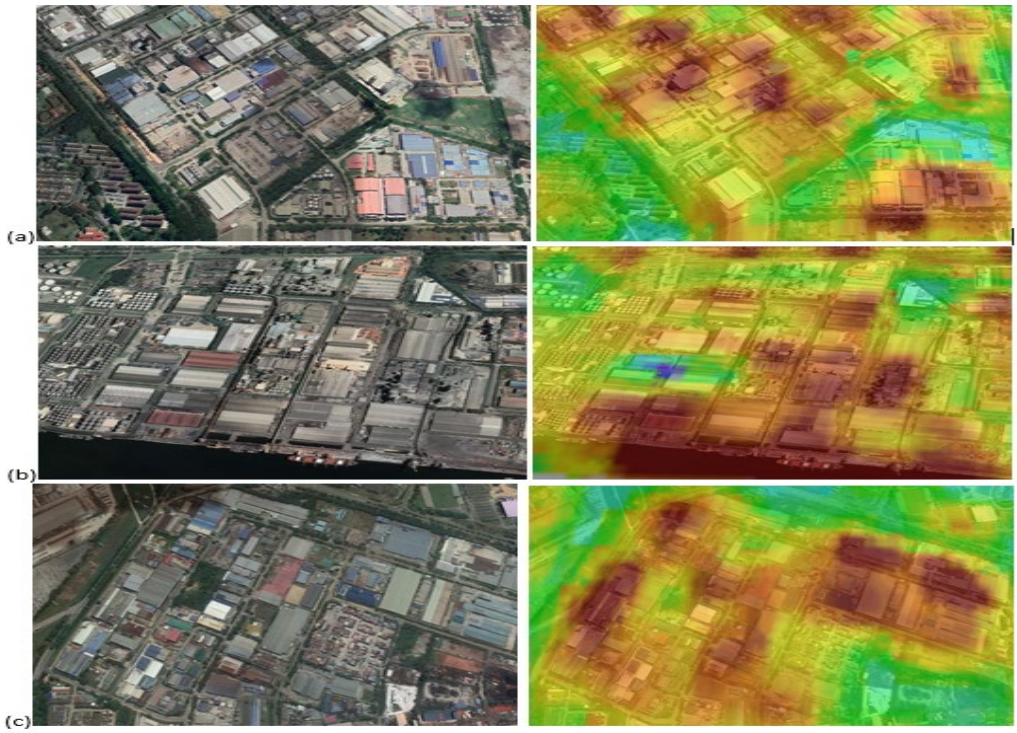

Figure 7. Heat sources from the Industries (a) Oil and gas (b) Chemicals (a) Sheet/Glass.

Table 4. LST and Emissivity values for the materials in the Pasir Gudang industrial area.

Material	Coordinate (° ′ ″)		Temp.°C	Emissivity
Lotte Chemical	1 26 04.91	103 54 26.78	49.77	0.972
Sheet/glass	1 27 04.12	103 55 25 91	49.68	0.971
Food processing	1 26 36.17	103 53 24.00	46.45	0.973
Oil and gas	1 27 30.94	103 53 57.83	49.16	0.976
Hitachi Chemicals	1 27 **0**4.29	103 54 38.52	48.91	0.971
Heng Hiap Industries	1 28 32.19	103 55 15.56	48.28	0.968
Lotte Chemical Titan.	1 28 31 34	103 55 15 10	50.21	0.968

5. Conclusion

The thermal heat mapping for estimating LST from Landsat8 TIR data in the Pasir Gudang industrial area has been successfully implemented. The thermal heat energy sources and other artificial surfaces (asphalt, roof sheeting) from the industrial plant from satellite sensors experienced high surface temperatures (>50°C), with accuracy (RMSE= $\pm$0.43°C). Vegetated covered surfaces including neighbouring agricultural areas marked the lowest temperatures (22~37 °C). The LST of selected targets have been validated using in-situ observation apart of comparison with corresponding downscaled MODIS LST product (MOD11A2), reporting a good agreement (R^2 0.78, $p < 0.001$). Hence, the approach adopted manifest as a relatively simple yet robust method in mapping industrial area thermal heat energy sources. Hence, mapping, and monitoring of industrial heat emission to support understanding toward improving disparities on existing industrial substances for policymakers and industrial developers to draft policies and regulations for relevant industries, most significantly it will help in fast-tracking Target 9.4. and 11.6. to retrofit industries to make them sustainable, with increased resource-use efficiency and reduce the environmental impact of cities, by paying special attention to air quality and waste management in municipal by 2030.

Acknowledgement
The authors wish to acknowledge the Ministry of Education Malaysia MRUN research grant (ref: PY/2019/02792), with vot number -RJ130000.7809.4L881 for this study. Facilities used at the Geoscience & Digital Earth Centre (INSTEG) and the Department of Geoinformatics Universiti of Teknologi Malaysia is highly commendable for this study. The Earth Resources Observation System (EROS), the data centre of the united states geological survey (USGS) and the National Aeronautics and Space Administration (NASA) are also acknowledged for the satellite data provided for this paper.

References
[1] S. Ferrari *et al.*, "Thermal infrared emissivity of felsic-rich to mafic-rich analogues of hot planetary regoliths," *Earth Planet. Sci. Lett.*, vol. **534,** p. 116089, 2020.
[2] A. B. Pour, M. Hashim, C. Makoundi, and K. Zaw, "Structural Mapping of the Bentong-Raub Suture Zone Using PALSAR Remote Sensing Data, Peninsular Malaysia: Implications for Sediment-hosted/Orogenic Gold Mineral Systems Exploration," *Resour. Geol.*, vol. **66,** no. 4, pp. 368–385, 2016.
[3] A. B. Pour, M. Hashim, J. K. Hong, and Y. Park, "Lithological and alteration mineral mapping in poorly exposed lithologies using Landsat-8 and ASTER satellite data: North-eastern Graham Land, Antarctic Peninsula," *Ore Geol. Rev.*, vol. **108,** pp. 112–133, 2019.
[4] M. Marghany, A. P. Cracknell, and M. Hashim, "Modification of fractal algorithm for oil spill detection from RADARSAT-1 SAR data," *Int. J. Appl. Earth Obs. Geoinf.*, vol. **11,** no. 2, pp. 96–102, 2009.
[5] S. Khorram, C. F. van der Wiele, F. H. Koch, S. A. C. Nelson, and M. D. Potts, *Principles of applied remote sensing*. 2016.
[6] S. M. Lee *et al.*, "Transport and diffusion of ozone in the nocturnal and morning planetary boundary layer of the Phoenix valley," *Environ. Fluid Mech.*, vol. 3, no. 4, pp. 331–362, 2003.
[7] A. Asgarian, B. J. Amiri, and Y. Sakieh, "Assessing the effect of green cover spatial patterns on urban land surface temperature using landscape metrics approach," *Urban Ecosyst.*, vol. **18,** no. 1, pp. 209–222, 2015.
[8] W. Zhou, J. Wang, and M. L. Cadenasso, "Effects of the spatial configuration of trees on urban heat mitigation: A comparative study," *Remote Sens. Environ.*, vol. 195, pp. 1–12, 2017.
[9] H. Takebayashi, "Influence of urban green area on air temperature of surrounding built-up area," *Climate*, vol. **5,** no. 3, 2017.
[10] J. Zawadzka *et al.*, "Downscaling Landsat-8 land surface temperature maps in diverse urban landscapes using multivariate adaptive regression splines and very high-resolution auxiliary data and very high-resolution auxiliary data," *Int. J. Digit. Earth*, vol. **0,** no. 0, pp. 1–16, 2019.
[11] S. Bonafoni and G. Tosi, "Downscaling of the land surface temperature using airborne high-resolution data: A case study on Aprilia, Italy," *IEEE Geosci. Remote Sens. Lett.*, vol. **14,** no. 1, pp. 1–5, 2017.
[12] J. Zawadzka, R. Corstanje, J. Harris, and I. Truckell, "Downscaling Landsat-8 land surface temperature maps in diverse urban landscapes using multivariate adaptive regression splines and very high-resolution auxiliary data," *Int. J. Digit. Earth*, vol. **0,** no. 0, pp. 1–16, 2019.
[13] K. Piikki and M. Söderström, "Digital soil mapping of arable land in Sweden – Validation of performance at multiple scales," *Geoderma*, vol. **352,** no. October 2017, pp. 342–350, 2019.
[14] L. J. Wang, M. Guo, K. Sawada, J. Lin, and J. Zhang, "Landslide susceptibility mapping in Mizunami City, Japan: A comparison between logistic regression, bivariate statistical analysis and multivariate adaptive regression spline models," *Catena*, vol. **135,** pp. 271–282, 2015.
[15] G. D. Jenerette *et al.*, "Micro-scale urban surface temperatures are related to land-cover features and residential heat-related health impacts in Phoenix, AZ USA," *Landsc. Ecol.*, vol. **31,** no. 4, pp. 745–760, 2016.
[16] B. A. Norton, A. M. Coutts, S. J. Livesley, R. J. Harris, A. M. Hunter, and N. S. G. Williams, "Planning for cooler cities: A framework to prioritise green infrastructure to mitigate high temperatures in urban landscapes," *Landsc. Urban Plan.*, vol. **134,** pp. 127–138, 2015.
[17] C. K. Yap, S. H. T. Peng, and C. S. Leow, "Contamination in Pasir Gudang Area, Peninsular Malaysia: What can we learn from Kim Kim River chemical waste contamination?," *J. Humanit. Educ. Dev.*, vol. **1,** no. 2, pp. 82–87, 2019.
[18] P. At, P. Gudang, P. Gudang, and J. D. Takzim, "Detailed Environmental Impact Assessment," no. October 2015.
[19] T. Wang *et al.*, "Recovering Land Surface Temperature Under Cloudy Skies Considering the Solar-Cloud-

Satellite Geometry: Application to MODIS and Landsat-8 Data," *J. Geophys. Res. Atmos.*, vol. **124,** no. 6, pp. 3401–3416, 2019.

[20] F. Wang, Z. Qin, C. Song, L. Tu, A. Karnieli, and S. Zhao, "An improved mono-window algorithm for land surface temperature retrieval from Landsat 8 thermal infrared sensor data," *Remote Sens.*, vol. **7,** no. 4, pp. 4268–4289, 2015.

[21] G. Rongali, A. K. Keshari, A. K. Gosain, and R. Khosa, "Split-Window Algorithm for Retrieval of Land Surface Temperature Using Landsat 8 Thermal Infrared Data," *J. Geovisualization Spat. Anal.*, vol. **2,** no. 2, 2018.

[22] J. A. Barsi, J. R. Schott, S. J. Hook, N. G. Raqueno, B. L. Markham, and R. G. Radocinski, "Landsat-8 thermal infrared sensor (TIRS) vicarious radiometric calibration," *Remote Sens.*, vol. **6,** no. 11, pp. 11607–11626, 2014.

[23] J. A. Smith, "Remote sensing of land surface temperature: the directional viewing effect," *IEEE Trans. Geosci. Remote Sens.*, vol. **35,** no. 4, pp. 972–974, 1997.

[24] M. S. Malik, J. P. Shukla, and S. Mishra, "Relationship of LST, NDBI and NDVI using Landsat-8 data in Kandaihimmat watershed, Hoshangabad, India," *Indian J. Geo-Marine Sci.*, vol. **48,** no. 1, pp. 25–31, 2019.

[25] J. C. Jimenez-Munoz, J. A. Sobrino, D. Skokovic, C. Mattar, and J. Cristobal, "Land surface temperature retrieval methods from Landsat-8 thermal infrared sensor data," *IEEE Geosci. Remote Sens. Lett.*, vol. **11,** no. 10, pp. 1840–1843, 2014.

[26] R. Algorithms, E. Models, and T. Implementation, "Land Surface Temperature Retrieval from Landsat 5, 7, and 8 over Rural Areas : Assessment of Different Retrieval Algorithms and Emissivity Models and Toolbox Implementation," 2020.

[27] H. Ren, C. Du, Q. Qin, R. Liu, J. Meng, and J. Li, "Atmospheric water vapour retrieval from Landsat 8 and its validation," *Int. Geosci. Remote Sens. Symp.*, pp. 3045–3048, 2014.

[28] A. Sekertekin and S. Bonafoni, "Land Surface Temperature Retrieval from Landsat 5, 7, and 8 over Rural Areas: Assessment of Different Retrieval Algorithms and Emissivity Models and Toolbox Implementation," *Remote Sens.*, vol. **12,** no. 2, p. 294, 2020.

[29] J. A. Sobrino *et al.*, "Land surface emissivity retrieval from different VNIR and TIR sensors," *IEEE Trans. Geosci. Remote Sens.*, vol. **46,** no. 2, pp. 316–327, 2008.

[30] Q. K. Nguyen, L. H. Trinh, K. H. Dao, and N. D. Dang, "Land Surface Temperature Dynamics In Dry Season 2015-2016 According To Landsat 8 Data In The South-East Region of Vietnam," *Geogr. Environ. Sustain.*, vol. **12,** no. 1, pp. 75–87, 2019.

[31] S. B. Duan *et al.*, "Land-surface temperature retrieval from Landsat 8 single-channel thermal infrared data in combination with NCEP reanalysis data and ASTER GED product," *Int. J. Remote Sens.*, vol. **40,** no. 5–6, pp. 1763–1778, 2019.

[32] L. Yang *et al.*, "Land surface temperature retrieval for arid regions based on Landsat-8 TIRS data: A case study in Shihezi, Northwest China," *J. Arid Land*, vol. **6,** no. 6, pp. 704–716, 2014.

[33] Y. Zhou, L. Zhang, J. Xiao, C. A. Williams, I. Vitkovskaya, and A. Bao, "Spatiotemporal transition of institutional and socioeconomic impacts on vegetation productivity in Central Asia over last three decades," *Sci. Total Environ.*, vol. **658,** pp. 922–935, 2019.

[34] Y. Jamei, P. Rajagopalan, and Q. (Chayn) Sun, "Spatial structure of surface urban heat island and its relationship with vegetation and built-up areas in Melbourne, Australia," *Sci. Total Environ.*, vol. **659,** pp. 1335–1351, 2019.

[35] Q. Weng, D. Lu, and J. Schubring, "Estimation of land surface temperature-vegetation abundance relationship for urban heat island studies," *Remote Sens. Environ.*, vol. **89,** no. 4, pp. 467–483, 2004.

[36] A. Bendib, H. Dridi, and M. I. Kalla, "Contribution of Landsat 8 data for the estimation of land surface temperature in Batna city, Eastern Algeria," *Geocarto Int.*, vol. **32,** no. 5, pp. 503–513, 2017.

[37] T. R. Oke, "The micrometeorology of the urban forest," *Philos. Trans. - R. Soc. London, B*, vol. **324,** no. 1223, pp. 335–349, 1989.